EXACT QUARK MASS CORRECTIONS TO HIGGS + JET PRODUCTION AT THE LHC*

Roberto Bonciani

Dipartimento di Fisica, Università di Roma "La Sapienza" and INFN Sezione di Roma
Piazzale Aldo Moro 2, 00185 Roma, Italy

Vittorio Del Duca

ETH Zürich, Institut für Theoretische Physik, 8093 Zürich, Switzerland
and
Physik-Institut, Universität Zürich, 8057 Zürich, Switzerland
and
INFN, Laboratori Nazionali di Frascati, 00044 Frascati (RM), Italy

Hjalte Frellesvig

Niels Bohr International Academy, University of Copenhagen
Blegdamsvej 17, 2100 Copenhagen, Denmark

Martijn Hidding

Department of Physics and Astronomy, Uppsala University
75120 Uppsala, Sweden

Valentin Hirschi

Theoretical Physics Department, CERN, 1211 Geneva 23, Switzerland

Francesco Moriello

DSM AG, Wurmisweg 576, 4303 Kaiseraugst, Switzerland

Giulio Salvatori

School of Natural Sciences, Institute for Advanced Study
Princeton, NJ, 08540, USA

Gábor Somogyi

HUN-REN Wigner Research Centre for Physics
Konkoly-Thege Miklós u. 29-33, 1121 Budapest, Hungary

Francesco Tramontano

Università di Napoli and INFN Sezione di Napoli
Complesso Universitario di Monte Sant'Angelo, Via Cintia, 80126 Napoli, Italy

Received 28 December 2023, accepted 5 January 2024,
published online 11 March 2024

* Presented at the XLV International Conference of Theoretical Physics "Matter to the Deepest", Ustroń, Poland, 17–22 September, 2023.

We present the computation of the next-to-leading order QCD corrections to the production of a Higgs boson in association with a jet at the LHC, including the exact dependence on the masses of quarks circulating in heavy-quark loops. The NLO corrections are computed including the top-quark mass as well as the bottom-quark mass. We show results in the on-shell and $\overline{\text{MS}}$ renormalisation schemes.

DOI:10.5506/APhysPolBSupp.17.2-A2

1. Introduction

The discovery of the Higgs boson by the ATLAS [1] and CMS [2] collaborations at the Large Hadron Collider (LHC) represents a spectacular confirmation of the Standard Model (SM) of elementary particles and is a milestone for particle physics. Currently, some of the main objectives of the experiments at the LHC are the precise determination of the couplings and quantum numbers of the Higgs boson. Since the detection of direct signals of beyond the Standard Model (BSM) physics has thus far eluded us at the LHC, such investigations are of paramount importance.

The main production channel for the Higgs boson at the LHC is via gluon fusion, with the coupling of the Higgs to gluons being mediated by a heavy-quark loop. This represents an excellent opportunity to both test the SM at the quantum level and to search for deviations from it. Indeed, the SM prediction is generally altered if new BSM particles are allowed to circulate in the loops, offering a possible gateway to the observation of New Physics (NP).

One promising observable to probe the BSM effects is the transverse momentum (p_{T}) distribution of the Higgs boson, which carries important information about the coupling of the Higgs boson to the virtual particles circulating in the loop. Moreover, in the boosted regime, it is possible to obtain a clean experimental signature for the Higgs decay products, making such studies even more appealing. Indeed, the theoretical description of the Higgs p_{T} distribution looks back on a rich history, with the exact leading order (LO) in α_{S} calculation with arbitrary internal fermion mass dating back to the late 1980s [3, 4]. Today, the Higgs p_{T} distribution is known at next-to-leading order (NLO) in α_{S} for the top-quark mass in the on-shell (OS) renormalisation scheme [5, 6]. Moreover, approximate NLO results including the bottom-quark mass [7–9] and the top–bottom interference [10] as well as predictions beyond NLO in the high-energy limit [11] have been presented in the literature. Mixed QCD-electroweak contributions to the Higgs p_{T} distribution have also been described in [12]. Furthermore, within Higgs Effective Field Theory (HEFT), the Higgs p_{T} distribution is known up to next-to-next-to-leading order (NNLO) in α_{S} [13–16].

In this contribution, we report on the calculation of the Higgs boson transverse momentum distribution at NLO in α_S, with exact top- and bottom-quark mass corrections. In our calculation, both the top- and bottom-quark masses are treated as dynamical parameters. Thus, we are able to compute predictions not only in the OS scheme, but also in a dynamical mass renormalisation scheme, the $\overline{\text{MS}}$ scheme, and study the scheme-dependence of the prediction.

2. Calculation

We consider the production of a Higgs boson in association with a jet in proton–proton collisions, $pp \to H + j + X$. The cross section for this process is obtained by convoluting the partonic cross sections for the three channels $gg \to Hg$, $q\bar{q} \to Hg$, and $q(\bar{q})g \to Hq(\bar{q})$ with the appropriate parton density functions (PDF). At LO in the strong coupling, these partonic processes involve one-loop $2 \to 2$ amplitudes, where the Higgs boson couples to a heavy quark running in the loop. In our computation, we treat the top and bottom quarks in loops as massive and retain the exact dependence of the results on their (arbitrary) masses.

At NLO in QCD, we must include one-loop $2 \to 3$ amplitudes that describe the production of the Higgs boson and jet together with an extra parton in the final state (real corrections), as well as $\mathcal{O}(\alpha_S)$ corrections to the $2 \to 2$ scattering amplitudes (virtual corrections). The necessary one-loop $2 \to 3$ diagrams are known analytically [17, 18], as well as numerically through public automated tools. In our calculation, we use the results of [18, 19] as reported in the MCFM-9.1 program [20]. We performed a cross-check of this implementation using the automated tools MG5_aMC@NLO [21, 22] and GoSam [23], finding perfect agreement for all phase-space points we compared, including those that approach an unresolved limit in the $2 \to 3$ kinematics.

The required $2 \to 2$ amplitudes can be written in terms of form-factors by exploiting their Lorentz and Dirac structures. For the $g(p_1) + g(p_2) \to g(p_3) + H(p_4)$ subprocess, we have

$$\mathcal{M}_{gg\to gH} = f^{c_1c_2c_3}\mathcal{S}_g^{\mu\nu\tau}\epsilon_{1,\mu}^{c_1}\epsilon_{2,\nu}^{c_2}\epsilon_{3,\tau}^{c_3}\,, \tag{1}$$

where $\mathcal{S}_g^{\mu\nu\tau}$ can be decomposed into four independent structures

$$\mathcal{S}_g^{\mu\nu\tau} = \mathcal{F}_1\,\mathcal{T}_{g,1}^{\mu\nu\tau} + \mathcal{F}_2\,\mathcal{T}_{g,2}^{\mu\nu\tau} + \mathcal{F}_3\,\mathcal{T}_{g,3}^{\mu\nu\tau} + \mathcal{F}_4\,\mathcal{T}_{g,4}^{\mu\nu\tau}\,. \tag{2}$$

Above c_1, c_2, and c_3 are the colour indices of the gluons $g(p_1)$, $g(p_2)$, and $g(p_3)$, and the tensor structures $\mathcal{T}_{g,i}^{\mu\nu\tau}$ read

$$\mathcal{T}^{\mu\nu\tau}_{g,1} = \frac{(s_{12}\, g^{\mu\nu} - 2p_2^\mu p_1^\nu)\,(s_{23}\, p_1^\tau - s_{13}\, p_2^\tau)}{2s_{13}}\,, \tag{3}$$

$$\mathcal{T}^{\mu\nu\tau}_{g,2} = \frac{(s_{23}\, g^{\nu\tau} - 2p_3^\nu p_2^\tau)\,(s_{13}\, p_2^\mu - s_{12}\, p_3^\mu)}{2s_{12}}\,, \tag{4}$$

$$\mathcal{T}^{\mu\nu\tau}_{g,3} = \frac{(s_{13}\, g^{\mu\tau} - 2p_3^\mu p_1^\tau)\,(s_{12}\, p_3^\nu - s_{23}\, p_1^\nu)}{2s_{23}}\,, \tag{5}$$

$$\begin{aligned}\mathcal{T}^{\mu\nu\tau}_{g,4} = \frac{1}{2}\,\{&g^{\mu\nu}\,(s_{23}p_1^\tau - s_{13}p_2^\tau) + g^{\nu\tau}\,(s_{13}p_2^\mu - s_{12}p_3^\mu)\\ &+g^{\tau\mu}\,(s_{12}p_3^\nu - s_{23}p_1^\nu) + 2p_1^\nu p_2^\tau p_3^\mu - 2p_1^\tau p_2^\mu p_3^\nu\}\,,\end{aligned} \tag{6}$$

with the following definitions of the Mandelstam invariants:

$$s_{12} = (p_1 + p_2)^2\,, \qquad s_{13} = (p_1 - p_3)^2\,, \qquad s_{23} = (p_2 - p_3)^2\,. \tag{7}$$

The form-factors can be extracted from Feynman diagrams using appropriate projection operators $\mathcal{P}^{\mu\nu\tau}_{g,i}$ that satisfy $\mathcal{P}^{\mu\nu\tau}_{g,i}\mathcal{S}_{g,\mu\nu\tau} = \mathcal{F}_i$.

Turning to the $q(p_1) + \bar{q}(p_2) \to g(p_3) + H(p_4)$ subprocess, we find

$$\mathcal{M}_{q\bar{q}\to gH} = t^{c_3}_{ij}\mathcal{S}^\tau_q \epsilon^{c_3}_{3,\tau}\,, \tag{8}$$

where $\mathcal{S}^\tau_q$ is the sum of just two independent structures

$$\mathcal{S}^\tau_q = \mathcal{G}_1\mathcal{T}^\tau_{q,1} + \mathcal{G}_2\mathcal{T}^\tau_{q,2}\,. \tag{9}$$

The tensor structures have the following form:

$$\mathcal{T}^\tau_{q,1} = p_1^\tau \not{p}_3 - \frac{1}{2}s_{13}\gamma^\tau\,, \tag{10}$$

$$\mathcal{T}^\tau_{q,2} = p_2^\tau \not{p}_3 - \frac{1}{2}s_{23}\gamma^\tau\,, \tag{11}$$

where the Mandelstam invariants s_{ij} are defined as above. Again, the form-factors can be extracted from Feynman diagrams by applying suitable projectors $\mathcal{P}^\tau_{q,i}$ that satisfy $\mathrm{Tr}(\mathcal{P}^\tau_{q,i}\mathcal{S}_{q,\tau}) = \mathcal{G}_i$.

The form-factors can be written in terms of scalar integrals that are divergent in four space-time dimensions. We use dimensional regularization in $d = 4-2\epsilon$ dimensions to regulate both UV and IR singularities. The obtained scalar integrals are then sorted into eight integral families and reduced to an independent set of master integrals (MIs) by solving integration-by-parts (IBP) identities using the computer programs FIRE [24, 25] and Kira [26, 27]. To compute the master integrals, we employed the method of differential equations. In this method, the MIs are expressed as the Laurent series in the parameter of dimensional regularization, $\epsilon = (4-d)/2$. Then, the set

of first-order linear differential equations satisfied by the MIs can be solved order-by-order in ϵ. In our calculation, we used the series-expansion method of [28] as implemented in the Mathematica package DiffExp [29] to solve the differential equations. The evaluation of all 447 MIs involved in the computation is described in detail in [30–32]. In order to check our results, we compared the numerical values of the full set of MIs in several phase-space points to values obtained with the numerical package AMFlow [33, 34]. In all cases, we found complete agreement with the requested full precision (16 digits).

Finally, the bare two-loop amplitudes must be renormalised. In order to understand the impact of using different renormalisation schemes for the internal quark masses, we considered three different setups differing in the radiative content and its treatment.

1. Top (OS): only the top quark is massive, the heavy-quark contribution is renormalised at zero momentum, the Yukawa coupling and heavy-quark mass are renormalised in the on-shell (OS) scheme.

2. Top ($\overline{\text{MS}}$): only the top quark is massive, the Yukawa coupling and heavy-quark mass are renormalised in the $\overline{\text{MS}}$ scheme.

3. Top+bottom($\overline{\text{MS}}$): the bottom quark is also included as a massive quark in all diagrams where it couples to the Higgs boson. For both the top and bottom quarks, the Yukawa couplings and heavy-quark masses are renormalised in the $\overline{\text{MS}}$ scheme.

In all three setups, we renormalise the external fields on-shell and the strong coupling in a mixed scheme where running always depends on five light flavours. Note that by retaining the bottom mass only in the loop where it couples to the Higgs boson, we can consistently use five-flavour running for α_S and five-flavour PDFs.

In order to validate our results for the $2 \to 2$ amplitudes, we examined their behaviour in the soft and collinear limits as one particle becomes unresolved. The form of the amplitude in these limits is given by one-loop infra-red (IR) factorization formulae in terms of lower-point amplitudes and universal soft and collinear functions [35–40]. Hence, we can generate a sequence of phase-space points tending to the desired limit and compare the value of the amplitude to that predicted by the corresponding IR factorization formula. We found that the amplitude approached the predicted limiting value with a rate expected from the cancellation of the leading singularity order-by-order in ϵ. Moreover, this behaviour was observed independently of the value of the internal-quark mass, as well as for the interference of

two massive internal quarks. As a further check, we verified that in the limit of very large transverse momentum, the full amplitude is in reasonable agreement with the approximated result of [41].

Finally, the IR singularities that remain after UV renormalisation of the amplitudes were regularized using the dipole subtraction method [42]. We used MCFM-9.1 [20] for the numerical evaluation of both the $2 \to 3$ amplitudes as well as the subtraction terms. We note that the phase-space integration of the $2 \to 3$ real-radiation contribution is not time-intensive even using automatically generated amplitudes. Nevertheless, employing the analytic results of [18, 19] results in a speed-up of about a hundred in the integration time of the gluonic $2 \to 3$ amplitude.

3. Results

Turning to our results, we begin by outlining our numerical setup. We consider proton–proton collisions at $\sqrt{s} = 13$ TeV and select events where the Higgs boson is produced in association with a jet. We use the anti-k_{T} algorithm [43] to reconstruct jets and demand that the leading jet have a transverse momentum larger than $p_{\mathrm{T}}^{j_1} > 20$ GeV. For our simulation, we use the value $G_{\mathrm{F}} = 1.16639 \times 10^{-5}$ GeV^{-2} for the Fermi constant and the NNPDF40_nlo_as_01180 [44] PDF set, which also fixes α_{S}. For the masses of the Higgs boson and heavy quarks, we choose $m_H = 125.25$ GeV and $m_t^{\mathrm{OS}} = 172.5$ GeV when employing the top (OS) setup. In the top ($\overline{\mathrm{MS}}$) and top+bottom ($\overline{\mathrm{MS}}$) setups, the values of the running top- and bottom-quark masses are computed by evolving them from $m_t^{\overline{\mathrm{MS}}}(m_t^{\overline{\mathrm{MS}}}) = 163.4$ GeV and $m_b^{\overline{\mathrm{MS}}}(m_b^{\overline{\mathrm{MS}}}) = 4.18$ GeV, respectively. We set the central renormalisation and factorisation scales to

$$\mu_{\mathrm{R}}^0 = \mu_{\mathrm{F}}^0 = \frac{H_{\mathrm{T}}}{2} = \frac{1}{2}\left(\sqrt{m_H^2 + p_{\perp,H}^2} + \sum_i |p_{\perp,i}|\right) \tag{12}$$

and perform a seven-point scale variation around this value to assess uncertainties.

Our results for the integrated cross section with the jet cuts given above are summarized in Table 1. Comparing LO and NLO results, we observe a large K-factor and a sizable reduction in scale uncertainty, from about 30% at LO to around 14% at NLO, in all three setups. Furthermore, we see that the top–bottom interference yields a negative contribution at LO. At NLO, this contribution is on the contrary positive and, in fact, offsets the difference between the cross sections with and without top–bottom interference.

Table 1. The cross section for Higgs boson production in association with a jet with transverse momentum larger than $p_{\mathrm{T}}^{j_1} > 20$ GeV at LO and NLO.

Renormalisation of internal masses	σ_{LO} [pb]	σ_{NLO} [pb]
top+bottom ($\overline{\mathrm{MS}}$)	$12.318^{+4.711}_{-3.117}$	$19.89(8)^{+2.84}_{-3.19}$
top ($\overline{\mathrm{MS}}$)	$12.538^{+4.822}_{-3.183}$	$19.90(8)^{+2.66}_{-2.85}$
top (OS)	$12.551^{+4.933}_{-3.244}$	$20.22(8)^{+3.06}_{-3.09}$

Turning to the transverse momentum distribution, in the left panel of figure 1, we plot the Higgs boson transverse momentum distribution in the top+bottom ($\overline{\mathrm{MS}}$) setup at LO and NLO. In order not to clutter the plot, we do not show distributions in the other setups, opting instead to highlight their behaviour in the next figures. Thus, in the right panel of figure 1, we show the NLO/LO ratio of the p_{T} distribution for all three renormalisation setups. We observe an almost flat K-factor of 2 in the top (OS) setup, with K-factors being slightly larger for the computations employing $\overline{\mathrm{MS}}$ renormalisation. We note that in contrast to what is observed at the inclusive level, the scale variation is the smallest in the top (OS) setup.

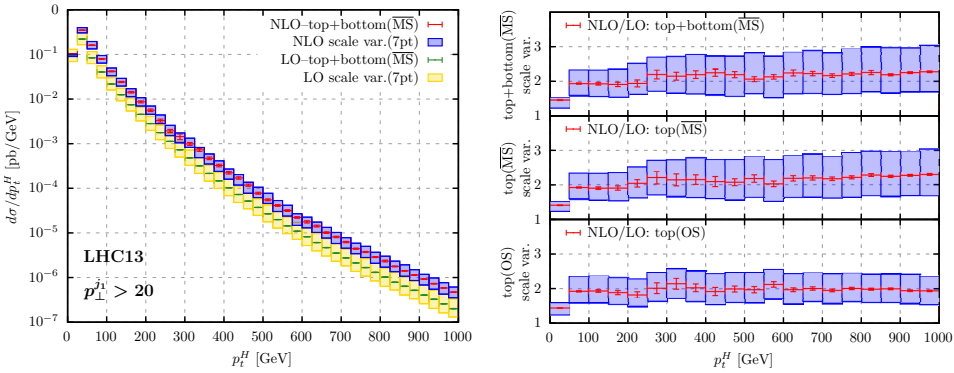

Fig. 1. The Higgs boson p_{T} distribution with top and bottom quarks (left) and NLO/LO ratio for the p_{T} distribution in all three setups (right).

Since the bottom quark is expected to affect the prediction only at small-to-intermediate values of the Higgs p_{T}, in figure 2, we show the p_{T} distribution at intermediate p_{T} values at LO (left) and NLO (right) for all three computational setups. Here, vertical bars represent the error from Monte Carlo integration. On the LO plot, the first bin is empty because the kinematic constraint $p_{\mathrm{T}} = p_{\mathrm{T}}^{j_1}$ forces the Higgs p_{T} to be larger than 20 GeV. In the next bin, we observe a negative contribution from top–bottom interference, while for $p_{\mathrm{T}} > 40$ GeV, the three computations yield basically the same

prediction. Turning to the NLO result, we observe that the top–bottom interference contribution produces a non-trivial change in the shape of the distribution at low p_{T}. It is negative in the first bin, positive in the second, then negative again and fades away for $p_{\mathrm{T}} > 60$ GeV. (We note thought that these differences are much smaller than those coming from scale variation.) It is also interesting to observe that the sensitivity of the prediction to the used renormalisation scheme increases as we go from LO to NLO.

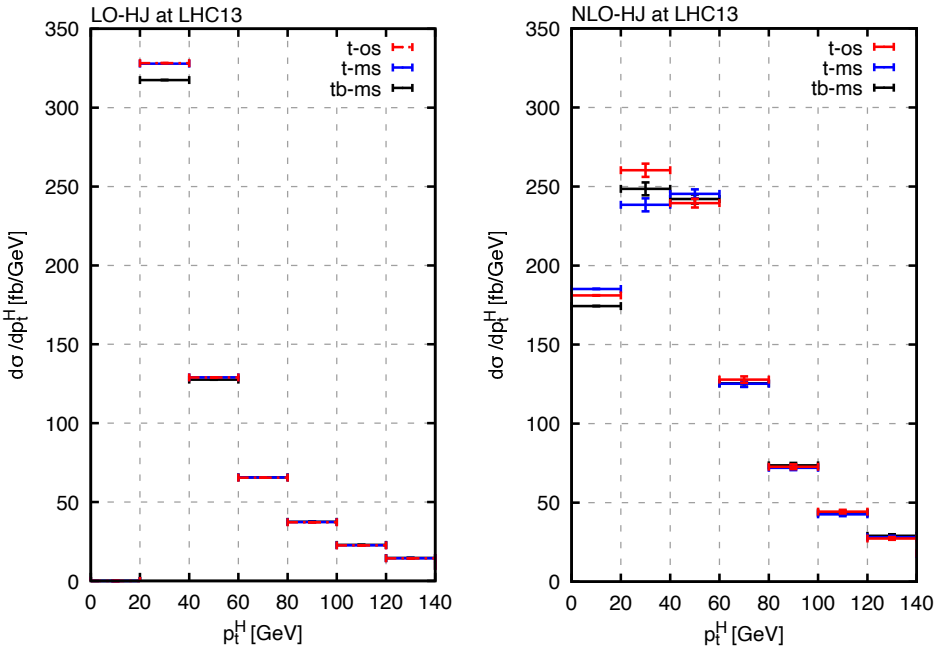

Fig. 2. The Higgs boson p_{T} distribution at intermediate p_{T} range at LO (left) and NLO (right).

Finally, in figure 3, we present ratio plots at LO (left) and NLO (right) for the Higgs transverse momentum distributions computed in the various renormalisation setups: top+bottom ($\overline{\mathrm{MS}}$) over top ($\overline{\mathrm{MS}}$) (upper panels), top (OS) over top+bottom ($\overline{\mathrm{MS}}$) (middle panels), and finally top (OS) over top ($\overline{\mathrm{MS}}$) (lower panels). Going from LO to NLO, we observe a nice reduction of scale uncertainty, represented here by the bands. Concurrently, we observe that the scheme dependence at large p_{T} is also significantly reduced at NLO. Moreover, as seen in the upper panels, the ratio of the distribution with top and bottom quarks to the distribution with top quarks only is flat and equal to 1, except for the very first bins. This highlights the fact that within scale uncertainty, the contribution of the bottom quark and of top–bottom interference to the Higgs p_{T} distribution is negligible, except at the

low end of the p_{T} spectrum. This then implies that the ratios in the middle and lower panels are basically equal. Last, we note that the p_{T} distribution falls off faster in the top ($\overline{\mathrm{MS}}$) setup than in the top (OS) setup. This is due to the fact that for large Higgs transverse momentum, the renormalisation scale μ_{R} in Eq. (12) increases with p_{T}, and so $m_t^{\overline{\mathrm{MS}}}(\mu_{\mathrm{R}})$ decreases.

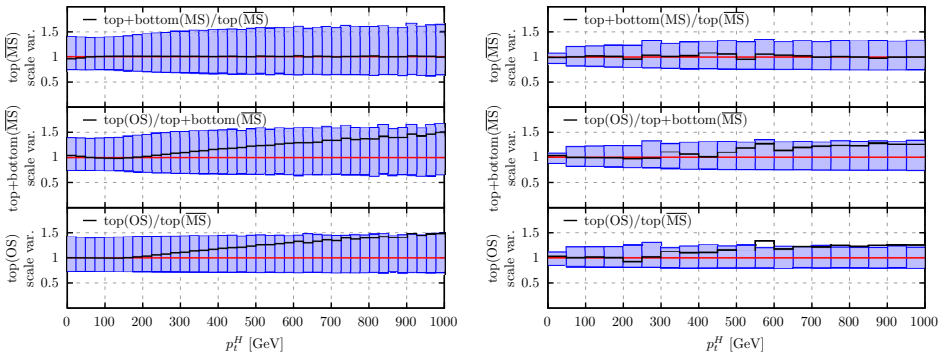

Fig. 3. Ratios of Higgs boson p_{T} distributions at LO (left) and NLO (right).

4. Conclusions

In this contribution, we have presented the rate for Higgs boson production in association with a hard jet at the LHC including NLO QCD corrections with top and bottom quarks circulating in the heavy-quark loops. Our computation is based on an evaluation of the necessary $2 \to 2$ amplitudes with arbitrary quark masses and thus allows for the use of dynamical mass renormalisation schemes, such as the $\overline{\mathrm{MS}}$ scheme. Thus, we are able to assess the exact impact of top–bottom interference as well as the choice of renormalisation scheme on observables such as the inclusive cross section or the Higgs boson transverse momentum distribution.

At the inclusive level, we observe that the top–bottom interference contribution at NLO is as large as the bottom-quark contribution at LO, however its sign is opposite. Thus, the bottom-quark effects in the inclusive cross section are almost completely erased at NLO. Nevertheless, bottom-quark effects do induce a non-trivial shape change of the Higgs p_{T} distribution at low p_{T}. On the other hand, in the hard tail of the distribution, a calculation neglecting bottom-quark effects is fully justified. Finally, we find that in the top-quark only calculation, the Higgs p_{T} distribution falls off faster in the $\overline{\mathrm{MS}}$ scheme than in the OS scheme at large p_{T}.

H.F. has received funding from the European Union's Horizon 2020 research and innovation program under the Marie Skłodowska-Curie grant agreement No. 847523 'INTERACTIONS', and has been partially supported by the Carlsberg Foundation Reintegration Fellowship. M.H. is supported by the European Research Council under ERC-STG-804286 UNISCAMP. R.B. is partly supported by the Italian Ministero della Università e della Ricerca (MIUR) under grant PRIN 20172LNEEZ. G.S. was supported by grant K 143451 of the National Research, Development and Innovation Fund in Hungary and by the Bolyai Fellowship programme of the Hungarian Academy of Sciences.

REFERENCES

[1] ATLAS Collaboration (G. Aad *et al.*), *Phys. Lett. B* **716**, 1 (2012).
[2] CMS Collaboration (S. Chatrchyan *et al.*), *Phys. Lett. B* **716**, 30 (2012).
[3] R.K. Ellis, I. Hinchliffe, M. Soldate, J.J. van der Bij, *Nucl. Phys. B* **297**, 221 (1988).
[4] U. Baur, E.W.N. Glover, *Nucl. Phys. B* **339**, 38 (1990).
[5] S.P. Jones, M. Kerner, G. Luisoni, *Phys. Rev. Lett.* **120**, 162001 (2018); *Erratum ibid.* **128**, 059901 (2022).
[6] X. Chen *et al.*, *J. High Energy Phys.* **2022**, 096 (2022).
[7] K. Melnikov, A. Penin, *J. High Energy Phys.* **2016**, 172 (2016).
[8] E. Braaten, H. Zhang, J.-W. Zhang, *Phys. Rev. D* **97**, 096014 (2018).
[9] F. Caola *et al.*, *J. High Energy Phys.* **2018**, 035 (2018).
[10] J.M. Lindert, K. Melnikov, L. Tancredi, C. Wever, *Phys. Rev. Lett.* **118**, 252002 (2017).
[11] F. Caola *et al.*, *J. High Energy Phys.* **2016**, 150 (2016).
[12] M. Becchetti *et al.*, *Phys. Rev. D* **103**, 054037 (2021).
[13] R. Boughezal *et al.*, *J. High Energy Phys.* **2013**, 072 (2013).
[14] X. Chen, T. Gehrmann, E.W.N. Glover, M. Jaquier, *Phys. Lett. B* **740**, 147 (2015).
[15] R. Boughezal *et al.*, *Phys. Rev. Lett.* **115**, 082003 (2015).
[16] R. Boughezal *et al.*, *Phys. Lett. B* **748**, 5 (2015).
[17] V. Del Duca *et al.*, *Nucl. Phys. B* **616**, 367 (2001).
[18] L. Budge *et al.*, *J. High Energy Phys.* **2020**, 079 (2020).
[19] R.K. Ellis, S. Seth, *J. High Energy Phys.* **2018**, 006 (2018).
[20] J. Campbell, T. Neumann, *J. High Energy Phys.* **2019**, 034 (2019).
[21] J. Alwall *et al.*, *J. High Energy Phys.* **2014**, 079 (2014).
[22] V. Hirschi, O. Mattelaer, *J. High Energy Phys.* **2015**, 146 (2015).
[23] G. Cullen *et al.*, *Eur. Phys. J. C* **74**, 3001 (2014).

[24] A.V. Smirnov, *J. High Energy Phys.* **2008**, 107 (2008).
[25] A.V. Smirnov, F.S. Chuharev, *Comput. Phys. Commun.* **247**, 106877 (2020).
[26] P. Maierhöfer, J. Usovitsch, P. Uwer, *Comput. Phys. Commun.* **230**, 99 (2018).
[27] J. Klappert, F. Lange, P. Maierhöfer, J. Usovitsch, *Comput. Phys. Commun.* **266**, 108024 (2021).
[28] F. Moriello, *J. High Energy Phys.* **2020**, 150 (2020).
[29] M. Hidding, *Comput. Phys. Commun.* **269**, 108125 (2021).
[30] R. Bonciani *et al.*, *J. High Energy Phys.* **2016**, 096 (2016).
[31] R. Bonciani *et al.*, *J. High Energy Phys.* **2020**, 132 (2020).
[32] H. Frellesvig *et al.*, *J. High Energy Phys.* **2020**, 093 (2020).
[33] X. Liu, Y.-Q. Ma, C.-Y. Wang, *Phys. Lett. B* **779**, 353 (2018).
[34] X. Liu, Y.-Q. Ma, *Comput. Phys. Commun.* **283**, 108565 (2023).
[35] Z. Bern, L.J. Dixon, D.C. Dunbar, D.A. Kosower, *Nucl. Phys. B* **425**, 217 (1994).
[36] Z. Bern, V. Del Duca, C. R. Schmidt, *Phys. Lett. B* **445**, 168 (1998).
[37] D.A. Kosower, *Nucl. Phys. B* **552**, 319 (1999).
[38] D.A. Kosower, P. Uwer, *Nucl. Phys. B* **563**, 477 (1999).
[39] Z. Bern, V. Del Duca, W.B. Kilgore, C.R. Schmidt, *Phys. Rev. D* **60**, 116001 (1999).
[40] S. Catani, M. Grazzini, *Nucl. Phys. B* **591**, 435 (2000).
[41] K. Kudashkin, K. Melnikov, C. Wever, *J. High Energy Phys.* **2018**, 135 (2018).
[42] S. Catani, M.H. Seymour, *Nucl. Phys. B* **485**, 291 (1997); *Erratum ibid.* **510**, 503 (1998).
[43] M. Cacciari, G.P. Salam, G. Soyez, *J. High Energy Phys.* **2008**, 063 (2008).
[44] NNPDF Collaboration (R.D. Ball *et al.*), *Eur. Phys. J. C* **82**, 428 (2022).